Noise-activated diffusion in the egg-carton potential

G. Caratti, R. Ferrando, R. Spadacini, and G. E. Tommei
Centro di Fisica delle Superfici e delle Basse Temperature del Consiglio Nazionale delle Ricerche and Istituto Nazionale di Fisica della Materia, Dipartimento di Fisica dell' Università di Genova, via Dodecaneso 33, 16146 Genova, Italy
(Received 20 February 1996)

The noise-activated diffusion of a classical particle in spatially periodic two-dimensional (2D) systems is studied by solving the corresponding Fokker-Planck equation. The particle is subjected to a periodic deterministic force, to a frictional force, and to a Gaussian white noise. The solution is obtained by extending to 2D the matrix-continued-fraction method for a quite general potential shape. The 2D diffusion coefficient is then numerically calculated for the square egg-carton potential; the analysis is performed over different friction and energy-barrier regimes. Several approximations are compared with the exact numerical results. In particular, the usual 1D diffusion-path approximation is discussed, showing that 2D effects are always present, becoming more and more relevant with decreasing friction. At high friction, a good analytical approximation is shown; on the contrary, none of the available approximations gives satisfactory results in intermediate- and low-damping regimes, which are typical in adatom diffusion on crystal surfaces. [S1063-651X(96)06711-6]

PACS number(s): 05.40.+j, 05.60.+w, 82.20.Fd

I. INTRODUCTION

Noise-activated diffusion in spatially periodic potentials is a topic of great interest in many scientific areas of physics, chemistry, and biophysics [1–3].

In recent years much effort has been devoted to the study of one-dimensional (1D) systems, in many different cases: Klein-Kramers equation, both at high and low friction [3–8], saw-tooth potentials [9], fluctuating barriers [10,11], and systems with time-dependent periodic perturbations [12]. Even in one dimension, the calculation of the relevant statistical quantities must be performed numerically, with the exception of limiting cases, where exact analytical results are usually available [13–15].

The Brownian motion in periodic potentials has been much less studied in multidimensional systems. The main results are approximated formulas for the diffusion coefficient at high friction [16] or at high-intermediate friction and high barriers [17]. More studied is the escape rate from multidimensional metastable or bistable wells; this problem has been studied in connection with the theory of chemical reactions both by analytical methods [18–20] and Langevin simulations [21]. The two-dimensional periodic case is of particular relevance, for example, in surface science where the adatom mobility in the surface plane controls the dynamics of many processes involving mass transport.

The main goal of this paper is the study of the Fokker-Planck dynamics of a classical particle in a two-dimensional coupled periodic potential. The particle is subjected to three forces: a periodic deterministic force, derived from the potential $V(\mathbf{r})$, a frictional force (η is the friction coefficient), and a white noise, related to the friction via the fluctuation-dissipation theorem [22]. In these conditions, the phase-space probability density f satisfies a four-variable Fokker-Planck equation (FPE), which is the Klein-Kramers equation in two-dimensional space:

$$\frac{\partial f}{\partial t} = -\mathbf{v}\cdot\frac{\partial f}{\partial \mathbf{r}} - \frac{\mathbf{F}(\mathbf{r})}{m}\cdot\frac{\partial f}{\partial \mathbf{v}} + \eta\frac{\partial}{\partial \mathbf{v}}\left(\mathbf{v}f + \frac{k_B T}{m}\frac{\partial f}{\partial \mathbf{v}}\right), \quad (1.1)$$

where $\mathbf{r}=(x,y)$, $\mathbf{v}=(v_x,v_y)$, and m are the position, the velocity, and the mass, $\mathbf{F}$ is the periodic deterministic force, T is the temperature, and η is the friction. In the presence of an x-y coupling in the potential, the dynamic problem cannot be separated into two independent one-dimensional problems, each giving a two-variable FPE.

The FPE will be solved by extending to four variables the matrix-continued-fraction method (MCFM) [3,23]. In this way, the Green function of the FPE and the dynamic structure factor S_s can be obtained. From S_s, the diffusion coefficient, the velocity correlation function, and the mean-square displacement may be computed via Kubo relations [22,24,25]. It has been recently shown that the jump rate and the probability distribution of the jump lengths in a periodic system can also be derived from S_s [7,26]. The method employed here is quite general; it can be applied to different lattices, position-dependent friction [6], tilted potentials [27], and memory friction [28]. In this paper we will analyze in detail the results concerning the diffusion coefficient D, in the case of a square lattice and of homogeneous friction. The potential $V(\mathbf{r})$ is chosen in the egg-carton shape (see Fig. 1)

$$V(x,y) = -2g_0(\cos x + \cos y) + 2g_1 \cos x \cos y.$$

The egg-carton potential depends on two parameters, g_0 and g_1, which give the amplitudes of the decoupled and coupled part, respectively. The egg-carton shape is the simplest choice in order to study genuine 2D effects. In fact at $g_1=0$ the potential is trivially decoupled and the 2D problem factorizes into two independent 1D problems; at $g_0=0$ the potential is again decoupled but rotated by $\pi/4$. The coupling term is responsible for the energy transfer between the x and y degrees of freedom and leads to qualitatively new dynamical features in the case of Hamiltonian systems. In these conservative systems, the motion in the egg-carton potential has been widely studied and regular and enhanced diffusion have been found depending on the strength of the x-y coupling and on the energy of the particle [29,30]. In

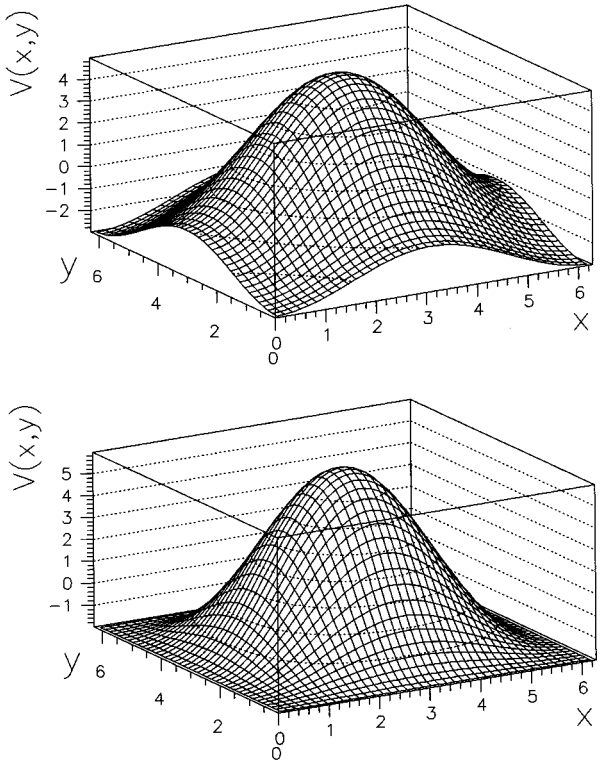

FIG. 1. The egg-carton potential in a lattice cell. The upper and lower panels correspond to $g_0=1$, $g_1=0.5$ and $g_0=1$, $g_1=1$, respectively. The latter case presents a flat channel.

order to model more realistic systems the noise has to be added; in the dissipative systems conventional diffusion always takes place, but the effects of the coupling may be relevant. In the dissipative regime, the diffusion coefficient has been calculated by Chen and Ying [31] for an anisotropic coupled potential of centered rectangular symmetry. Here we study the egg-carton potential where the amplitude of the diffusion barriers and the strength of the x-y coupling can be easily and independently changed.

For simplicity, diffusion is usually treated in the 1D picture, here named ''diffusion-path approximation'' (DPA), obtained by considering the most probable diffusion path connecting the minima via the saddle points. Our first goal is then the investigation of possible dimensional effects, by comparison between our 2D exact results and 1D treatments. The topic is particularly important, for example, in surface diffusion at crystals. As shown by the authors [6,32,33], the FPE can describe the diffusion at crystals in every friction and barrier regime, from energy-controlled to spatial-controlled diffusion and from activated to unactivated diffusion. In principle the DPA can be calculated at every friction. Then, by solving the FPE in a wide damping range, dimensional effects are studied both at high- and low-friction values. The importance of the low- and intermediate-damping regimes has been recently highlighted by many experimental and theoretical works on surface diffusion [6,33–41].

The exact numerical calculations will be compared also with two different approximations whose validity is restricted to limited parameter ranges.

At high friction, in the Smoluchowski limit, a ''quasi-2D'' approximation is derived in the framework of the linear response theory. The diffusion coefficient (along the x direction, for instance) in the quasi-2D approximation is obtained by generalizing to two dimensions the method presented by Günther *et al.* [15] for deriving the exact 1D result [14].

At intermediate and low friction, the numerical results will be compared to those of the 2D-jump model [42]. In the latter model, the diffusion coefficient is expressed by $D=\frac{1}{4}\langle l^2\rangle r_j$, $\langle l^2\rangle$ being the mean-square jump length, and r_j the total jump rate. Activated diffusion is assumed and then the validity of the picture is restricted to high potential barriers. A simple evaluation of $\langle l^2\rangle$ is possible if the damping is not too low. In this regime, the diffusion proceeds only by single jumps [25,33] and the mean-square displacement is given by a^2, where a is the lattice spacing. Following Langer [17,18,43], the rate is calculated as a 2D extension of Kramers's [44] result in the spatially limited diffusion regime.

The paper is organized as follows. In Sec. II the 2D MCFM is outlined for a general coupled potential $V(\mathbf{r})$. Section III contains a brief description of the potential actually used in the numerical calculations. Section IV contains the results; in subsection A the Smoluchowski limit is considered, whereas subsection B deals with the intermediate- and low-friction regimes. The conclusions are outlined in Sec. V.

II. THE MATRIX-CONTINUED-FRACTION METHOD

In this section the MCFM [3,23] is first extended to the 2D case to obtain the time-dependent solution of the FPE [Eq. (1.1)] in a coupled periodic potential $V(\mathbf{r})$.

A square lattice of spacing a and homogeneous friction η are here considered for simplicity and, as in the 1D case [25], the following dimensionless variables are introduced:

$$\overline{\mathbf{r}}=\frac{2\pi}{a}\mathbf{r},\quad \overline{t}=\frac{2\pi}{a}\sqrt{\frac{k_BT}{m}}t,\quad \overline{\mathbf{v}}=\sqrt{\frac{m}{k_BT}}\mathbf{v},$$

$$\gamma=\frac{a}{2\pi}\sqrt{\frac{m}{k_BT}}\eta,\quad \overline{V(\overline{\mathbf{r}})}=\frac{V(\mathbf{r})}{k_BT},\quad \overline{\mathbf{F}(\overline{\mathbf{r}})}=\frac{a}{2\pi}\frac{\mathbf{F}(\mathbf{r})}{k_BT}. \tag{2.1}$$

With this choice for $\mathbf{r}$, the unit cell goes from $-\pi$ to π and from $-1/2$ to $+1/2$ in the real and reciprocal axes, respectively. In the following the dimensionless variables in Eq. (2.1) will be rewritten without overline and in the FPE,

$$\frac{\partial f(\mathbf{r},\mathbf{v},t)}{\partial t}=L_{\mathrm{FP}}f(\mathbf{r},\mathbf{v},t), \tag{2.2}$$

the Fokker-Planck (FP) operator becomes

$$L_{\mathrm{FP}}=-\mathbf{v}\cdot\frac{\partial}{\partial\mathbf{r}}-\mathbf{F}(\mathbf{r})\cdot\frac{\partial}{\partial\mathbf{v}}+\gamma\frac{\partial}{\partial\mathbf{v}}\cdot\left(\mathbf{v}+\frac{\partial}{\partial\mathbf{v}}\right). \tag{2.3}$$

Let us introduce now the operators

$$D=\frac{\partial}{\partial x}+\frac{1}{2}F_x(\mathbf{r}),\quad \hat{D}=\frac{\partial}{\partial x}-\frac{1}{2}F_x(\mathbf{r}),$$

$$\Delta=\frac{\partial}{\partial y}+\frac{1}{2}F_y(\mathbf{r}),\quad \hat{\Delta}=\frac{\partial}{\partial y}-\frac{1}{2}F_y(\mathbf{r}),$$

$$b=\frac{\partial}{\partial v_x}+\frac{1}{2}v_x,\quad b^\dagger=-\frac{\partial}{\partial v_x}+\frac{1}{2}v_x,$$

$$\beta=\frac{\partial}{\partial v_y}+\frac{1}{2}v_y,\quad \beta^\dagger=-\frac{\partial}{\partial v_y}+\frac{1}{2}v_y, \tag{2.4}$$

where b and $b^\dagger$, as well as β and $\beta^\dagger$, are the well-known annihilation and creation operators for the harmonic oscillator in quantum mechanics, corresponding to the variables v_x or v_y, respectively. It is useful to recall the properties of these operators when applied to harmonic oscillator eigenfunctions $\psi_n(v)$:

$$b^\dagger b\,\psi_n(v)=n\,\psi_n(v),\quad b^\dagger\psi_n(v)=\sqrt{n+1}\,\psi_{n+1}(v),$$

$$b\,\psi_n(v)=\sqrt{n}\,\psi_{n-1}(v),\quad \psi_n(v)=\frac{(b^\dagger)^n}{\sqrt{n!}}\psi_0(v),$$

$$\psi_0(v)=\frac{1}{(2\pi)^{1/4}}\exp\left(-\frac{v^2}{4}\right). \tag{2.5}$$

With the aid of definitions (2.4) the FP operator can be rewritten as

$$L_{\mathrm{FP}}=-\psi_0(v_y)\psi_0(v_x)\exp\left(-\frac{V(\mathbf{r})}{2}\right)\{bD+b^\dagger\hat{D}+\beta\Delta+\beta^\dagger\hat{\Delta}$$
$$+\gamma b^\dagger b+\gamma\beta^\dagger\beta\}\exp\left(\frac{V(\mathbf{r})}{2}\right)\psi_0^{-1}(v_y)\psi_0^{-1}(v_x). \tag{2.6}$$

The dynamic structure factor S_s is the Fourier transform with respect to time of the characteristic function Σ_s [24]. The latter can be calculated if one knows the stationary probability density P_{st} and the conditional probability density P_c:

$$\Sigma_s(\mathbf{q},t)=\int_{-\infty}^{\infty}dv_x\int_{-\infty}^{\infty}dv_y\int_{-\infty}^{\infty}dv_{0x}\int_{-\infty}^{\infty}dv_{0y}\int_{-\pi}^{\pi}dx_0$$
$$\times\int_{-\pi}^{\pi}dy_0\int_{-\infty}^{\infty}dx\int_{-\infty}^{\infty}dy\,P_{\mathrm{st}}(\mathbf{r}_0,\mathbf{v_0})$$
$$\times P_c(\mathbf{r},\mathbf{v},t/\mathbf{r}_0,\mathbf{v}_0,0)\exp[-i\mathbf{q}\cdot(\mathbf{r}-\mathbf{r}_0)]. \tag{2.7}$$

The Boltzmann distribution

$$P_{\mathrm{st}}(\mathbf{r}_0,\mathbf{v}_0)=\frac{1}{N}\psi_0^2(v_{0x})\psi_0^2(v_{0y})\exp[-V(\mathbf{r}_0)], \tag{2.8}$$

with

$$N=\int_{-\pi}^{\pi}dx\int_{-\pi}^{\pi}dy\exp[-V(\mathbf{r})], \tag{2.9}$$

satisfies the required normalization condition

$$\int_{-\infty}^{\infty}dv_x\int_{-\infty}^{\infty}dv_y\int_{-\pi}^{\pi}dx\int_{-\pi}^{\pi}dy\,P_{\mathrm{st}}(\mathbf{r},\mathbf{v})=1. \tag{2.10}$$

The conditional probability $P_c(\mathbf{r},\mathbf{v},t/\mathbf{r}_0,\mathbf{v}_0,0)$ of having the particle in $\mathbf{r},\mathbf{v}$ at time t, if it was in $\mathbf{r}_0,\mathbf{v}_0$ at time 0, is the Green function of the probability density $f(\mathbf{r},\mathbf{v},t)$, that means the solution of the FPE [Eq. (2.2)] with initial δ condition in both position and velocity.

The nonperiodic time-dependent solution of the FPE can be expanded in Bloch functions as

$$f(\mathbf{r},\mathbf{v},t)=\int_{-1/2}^{1/2}dk_x\int_{-1/2}^{1/2}dk_y\tilde{f}(\mathbf{k},\mathbf{r},\mathbf{v},t)\exp(i\mathbf{k}\cdot\mathbf{r}), \tag{2.11}$$

where $\tilde{f}$ is a periodic function of $\mathbf{r}$; then $\tilde{f}(\mathbf{k},\mathbf{r},\mathbf{v},t)$ is further expanded in Fourier series as for space variables and in Hermite functions $\psi_m(v_x)$, $\psi_n(v_y)$ as for velocity variables:

$$\tilde{f}(\mathbf{k},\mathbf{r},\mathbf{v},t)=\frac{1}{2\pi}\psi_0(v_x)\psi_0(v_y)\exp\left(-\frac{V(\mathbf{r})}{2}\right)$$
$$\times\sum_{p,h=-\infty}^{\infty}\sum_{m,n=0}^{\infty}c_m^{phn}(\mathbf{k},t)\psi_m(v_x)\psi_n(v_y)$$
$$\times\exp(ipx)\exp(ihy). \tag{2.12}$$

In order to obtain a solution of the FPE with initial δ condition, it is sufficient to impose that

$$\tilde{f}(\mathbf{k},\mathbf{r},\mathbf{v},0)\exp(i\mathbf{k}\cdot\mathbf{r})=\delta(\mathbf{r}-\mathbf{r}_0)\,\delta(\mathbf{v}-\mathbf{v}_0). \tag{2.13}$$

Consequently, the coefficients c of Eq. (2.12) at time $t=0$ have the following form:

$$c_m^{phn}(\mathbf{k},0)=\frac{1}{2\pi}\frac{\psi_m(v_{0x})\psi_n(v_{0y})}{\psi_0(v_{0x})\psi_0(v_{0y})}\exp\left(\frac{V(\mathbf{r}_0)}{2}\right)\exp[-i(p$$
$$+k_x)x_0]\exp[-i(h+k_y)y_0]. \tag{2.14}$$

The coefficients at time t can be connected with the coefficients at time $t=0$ introducing the functions G:

$$c_m^{phn}(\mathbf{k},t)=\sum_{i,j=0}^{\infty}\sum_{r,s=-\infty}^{\infty}G_{mi}^{phnrsj}(\mathbf{k},t)c_i^{rsj}(\mathbf{k},0). \tag{2.15}$$

Using Eqs. (2.11), (2.12), (2.14), and (2.15), the result for the conditional probability is

$$P_c(\mathbf{r},\mathbf{v},t/\mathbf{r}_0,\mathbf{v}_0,0)=\frac{1}{4\pi^2}\frac{\psi_0(v_x)\psi_0(v_y)\exp[-V(\mathbf{r})/2]}{\psi_0(v_{0x})\psi_0(v_{0y})\exp[-V(\mathbf{r}_0)/2]}\sum_{m,n=0}^{\infty}\sum_{i,j=0}^{\infty}\psi_i(v_{0x})\psi_j(v_{0y})\psi_m(v_x)\psi_n(v_y)$$
$$\times\int_{-1/2}^{1/2}dk_x\int_{-1/2}^{1/2}dk_y\sum_{p,h=-\infty}^{\infty}\sum_{r,s=-\infty}^{\infty}\exp[-i(r+k_x)x_0]\exp[-i(s+k_y)y_0]$$
$$\times\exp[i(p+k_x)x]\exp[i(h+k_y)y]G_{mi}^{phnrsj}(\mathbf{k},t). \tag{2.16}$$

Inserting Eqs. (2.8) and (2.16) in Eq. (2.7) we get

$$\Sigma_s(\mathbf{q},t)=\frac{1}{4\pi^2N}\sum_{p,h=-\infty}^{\infty}\sum_{r,s=-\infty}^{\infty}G_{00}^{ph0rs0}(\boldsymbol{\xi},t)M_{p-l_x,h-l_y}M^*_{r-l_x,s-l_y}, \tag{2.17}$$

where $\mathbf{q}=(q_x,q_y)=(\xi_x+l_x,\xi_y+l_y)$, $-1/2<\xi_x\leqslant 1/2$, $-1/2<\xi_y\leqslant 1/2$, and l_x, l_y are integers, and

$$M_{ph}=\int_{-\pi}^{\pi}dx\int_{-\pi}^{\pi}dy\exp\left(-\frac{V(\mathbf{r})}{2}\right)\exp(ipx)\exp(ihy). \tag{2.18}$$

In Eq. (2.17) only the G functions having $n=m=i=j=0$ are involved due to the orthonormalization properties of the Hermite functions. If $V(\mathbf{r})$ is an even function of both x and y, all the integrals M_{ph} are real.

The Laplace transform $\tilde{S}_s(\mathbf{q},z)$ of the characteristic function $\Sigma_s(\mathbf{q},t)$ then takes the form

$$\tilde{S}_s(\mathbf{q},z)=\frac{1}{4\pi^2N}\sum_{p,h=-\infty}^{\infty}\sum_{r,s=-\infty}^{\infty}\tilde{G}_{00}^{ph0rs0}(\xi,z)M_{p-l_x,h-l_y}M^*_{r-l_x,s-l_y}. \tag{2.19}$$

$\Sigma_s(\mathbf{q},t)$ being an even function of time, the dynamic structure factor $S_s(\mathbf{q},\omega)$ is given by

$$S_s(\mathbf{q},\omega)=\frac{1}{\pi}\mathrm{Re}\{\tilde{S}_s(\mathbf{q},i\omega)\}, \tag{2.20}$$

and we finally obtain

$$S_s(\mathbf{q},\omega)=\frac{1}{4\pi^3N}\mathrm{Re}\left\{\sum_{p,h=-\infty}^{\infty}\sum_{r,s=-\infty}^{\infty}\tilde{G}_{00}^{ph0rs0}(\xi,z)M_{p-l_x,h-l_y}M^*_{r-l_x,s-l_y}\right\}, \tag{2.21}$$

with $z=i\omega$.

In the following we derive a recurrence relation for the $\tilde{G}_{00}^{ph0rs0}(\xi,z)$. As a first step, we insert Eqs. (2.11) and (2.12) in Eq. (2.2) and using Eqs. (2.5) and (2.6) we get an equation for the coefficients c:

$$\frac{\partial c_m^{rsj}(\mathbf{k},t)}{\partial t}=\sum_{n=0}^{\infty}\sum_{p,h=-\infty}^{\infty}\{Q_m^{(-)rsjphn}c_{m-1}^{phn}(\mathbf{k},t)+Q_m^{rsjphn}c_m^{phn}(\mathbf{k},t)+Q_m^{(+)rsjphn}c_{m+1}^{phn}(\mathbf{k},t)\}, \tag{2.22}$$

where

$$Q_m^{rsjphn}=\frac{1}{4\pi^2}\int_{-\infty}^{\infty}dv_y\int_{-\pi}^{\pi}dx\int_{-\pi}^{\pi}dy\,\psi_j(v_y)\exp[-i(r+k_x)x]$$
$$\times\exp[-i(s+k_y)y]Q_m\psi_n(v_y)\exp[i(p+k_x)x]\exp[i(h+k_y)y],$$
$$Q_m^{(\pm)rsjphn}=\frac{1}{4\pi^2}\int_{-\infty}^{\infty}dv_y\int_{-\pi}^{\pi}dx\int_{-\pi}^{\pi}dy\,\psi_j(v_y)\exp[-i(r+k_x)x]\exp[-i(s+k_y)y]Q_m^{(\pm)}\psi_n(v_y)$$
$$\times\exp[i(p+k_x)x]\exp[i(h+k_y)y], \tag{2.23}$$

and

$$Q_m=-(m\gamma+\beta\Delta+\beta^\dagger\hat{\Delta}+\gamma\beta^\dagger\beta),$$
$$Q_m^{(-)}=-\sqrt{m}\hat{D},\quad Q_m^{(+)}=-\sqrt{m+1}D. \tag{2.24}$$

In obtaining Eq. (2.22), the properties of the operators defined in Eqs. (2.4) have been applied to $\psi_m(v_x)$, while the sum on n index is still present; as it will be clear in the following, this is one way for getting a tridiagonal recurrence relationship. Inserting Eq. (2.24) in (2.23) and remembering the definitions of the operators (2.4) and the properties (2.5), Q, $Q^{(+)}$, and $Q^{(-)}$ can be written as

$$Q_m^{rsjphn} = -\gamma(n+m)\,\delta^{pr}\delta^{hs}\delta^{jn} - i(h+k_y)\,\delta^{pr}\delta^{hs}[\sqrt{n}\,\delta^{j,n-1} + \sqrt{n+1}\,\delta^{j,n+1}] - \tfrac{1}{2}F_y^{p-r,h-s}[\sqrt{n}\,\delta^{j,n-1} - \sqrt{n+1}\,\delta^{j,n+1}],$$

$$Q_m^{(-)rsjphn} = -\sqrt{m}\,\delta^{jn}[i(p+k_x)\,\delta^{pr}\delta^{hs} - \tfrac{1}{2}F_x^{p-r,h-s}],$$

$$Q_m^{(+)rsjphn} = -\sqrt{m+1}\,\delta^{jn}[i(p+k_x)\,\delta^{pr}\delta^{hs} + \tfrac{1}{2}F_x^{p-r,h-s}] \tag{2.25}$$

if we define

$$F_y^{p-r,h-s} = \frac{1}{4\pi^2}\int_{-\pi}^{\pi}dx\int_{-\pi}^{\pi}dy F_y(\mathbf{r})\exp[i(p-r)x] \times \exp[i(h-s)y],$$

$$F_x^{p-r,h-s} = \frac{1}{4\pi^2}\int_{-\pi}^{\pi}dx\int_{-\pi}^{\pi}dy F_x(\mathbf{r})\exp[i(p-r)x] \times \exp[i(h-s)y]. \tag{2.26}$$

$F_x(\mathbf{r})$ and $F_y(\mathbf{r})$, and consequently Q, $Q^{(+)}$, and $Q^{(-)}$, are completely determined by the potential $V(\mathbf{r})$.

Inserting Eq. (2.15) in Eq. (2.22) one obtains a corresponding recurrence relation for the G functions:

$$\frac{\partial G_{mi}^{phnrsj}(\mathbf{k},t)}{\partial t} = \sum_{d=0}^{\infty}\sum_{a,b=-\infty}^{\infty}\{Q_m^{(-)phnabd}G_{m-1,i}^{abdrsj}(\mathbf{k},t) + Q_m^{phnabd}G_{mi}^{abdrsj}(\mathbf{k},t) + Q_m^{(+)phnabd}G_{m+1,i}^{abdrsj}(\mathbf{k},t)\}. \tag{2.27}$$

The indices p, h, r, and s are integers varying between $-\infty$ and ∞ whereas the integers n, j vary between 0 and ∞. In order to obtain a numerical result, it is necessary to truncate the recurrence relation, i.e., to choose P, H, R, S, N, and J so that

$$-P \leqslant p \leqslant P, \quad -H \leqslant h \leqslant H, \quad 0 \leqslant n \leqslant N,$$

$$-R \leqslant r \leqslant R, \quad -S \leqslant s \leqslant S, \quad 0 \leqslant j \leqslant J. \tag{2.28}$$

Eq. (2.27) can be identified with a tridiagonal relationship [25] if the objects labeled by (p, h, n) and (r, s, j) are rearranged according to two indices u and v [28]; a possible rearrangement is

$$u = (h+H)(2P+1) + (p+P+1) + n(2P+1)(2H+1),$$

$$v = (s+S)(2R+1) + (r+R+1) + j(2R+1)(2S+1), \tag{2.29}$$

and a similar rearrangement is introduced for the summed up indices. Taking

$$(p,h,n) \to u, \quad (r,s,j) \to v, \quad (a,b,d) \to w,$$

Eq. (2.27) can in fact be written as

$$\frac{\partial G_{mi}^{uv}(\mathbf{k},t)}{\partial t} = \sum_{w}\{Q_m^{(-)uw}G_{m-1,i}^{wv}(\mathbf{k},t) + Q_m^{uw}G_{mi}^{wv}(\mathbf{k},t) + Q_m^{(+)uw}G_{m+1,i}^{wv}(\mathbf{k},t)\}. \tag{2.30}$$

The upper indices label the matrix elements whereas the lower ones label the matrices. In matrix notation, one obtains the following tridiagonal recurrence relationship for the matrix $\underline{G}$:

$$\frac{\partial \underline{G}_{mi}(\mathbf{k},t)}{\partial t} = \underline{Q}_m^{(-)}\underline{G}_{m-1,i}(\mathbf{k},t) + \underline{Q}_m\underline{G}_{mi}(\mathbf{k},t) + \underline{Q}_m^{(+)}\underline{G}_{m+1,i}(\mathbf{k},t). \tag{2.31}$$

Considering the Laplace transform of Eq. (2.31) with $i=0$, one obtains

$$z\underline{\widetilde{G}}_{m0}(\mathbf{k},z) - \underline{G}_{m0}(\mathbf{k},0) = \underline{Q}_m^{(-)}\underline{\widetilde{G}}_{m-1,0}(\mathbf{k},z) + \underline{Q}_m\underline{\widetilde{G}}_{m0}(\mathbf{k},z) + \underline{Q}_m^{(+)}\underline{\widetilde{G}}_{m+1,0}(\mathbf{k},z), \tag{2.32}$$

which can be solved by standard methods [3]. The solution is written as a continued fraction,

$$\underline{\widetilde{G}}_{00}(\mathbf{k},z) = (z\underline{I} + \underline{B} - \underline{B}^{(+)}\{z\underline{I} + \underline{A} + \underline{B} - 2\underline{B}^{(+)}[z\underline{I} + 2\underline{A} + \underline{B} - 3\underline{B}^{(+)} \times (z\underline{I} + 3\underline{A} + \underline{B} - \cdots)^{-1}\underline{B}^{(-)}]^{-1}\underline{B}^{(-)}\}^{-1}\underline{B}^{(-)})^{-1}, \tag{2.33}$$

where the matrices $\underline{B}^{(-)}$, $\underline{B}^{(+)}$, $\underline{B}$ are defined as

$$\underline{Q}_m^{(-)} = -\sqrt{m}\,\underline{B}^{(-)},$$

$$\underline{Q}_m^{(+)} = -\sqrt{m+1}\,\underline{B}^{(+)},$$

$$\underline{Q}_m = -m\underline{A} - \underline{B}, \tag{2.34}$$

$\underline{A}$ is the matrix obtained by rearranging the indices of

$$A^{phnrsj} = \gamma \delta^{pr} \delta^{hs} \delta^{nj}, \tag{2.35}$$

and $\underline{I}$ is the identity matrix.

From Eq. (2.33) it is possible to obtain all the $\tilde{G}_{00}^{ph0rs0}$ in the expression of the dynamic structure factor [Eq. (2.21)].

If the 2D potential $V(x,y)$ is decoupled [$V(x,y) = V_1(x) + V_2(y)$], the 2D problem factorizes into two 1D independent problems. The 1D problem has been treated in detail in a previous work by the same authors [25].

In a square lattice, the diffusion tensor is isotropic, so only one diffusion coefficient is to be considered. The latter can be derived from the well-known Green-Kubo relationship [24]:

$$D = \pi \lim_{\omega \to 0} \omega^2 \lim_{q \to 0} \frac{S_s(\mathbf{q}, \omega)}{q^2}, \tag{2.36}$$

where $q = \sqrt{q_x^2 + q_y^2}$, and, with no loss of generality, D can be evaluated for diffusion along the x axis, i.e., at $q_y = 0$.

III. THE 2D COUPLED POTENTIAL

In the following we present the explicit results for the egg-carton potential:

$$V(x,y) = -2g_0(\cos x + \cos y) + 2g_1 \cos x \cos y. \tag{3.1}$$

Dimensionless units are employed and the potential is normalized as in Eq. (2.1). This model potential, which looks like an egg carton, has a square symmetry and is often introduced in the study of the nonlinear dynamics of a classical particle moving conservatively in a periodic field of force [29,30]. At $g_1 = 0$ the potential is trivially decoupled; at $g_0 = 0$ the potential is again decoupled but rotated by $\pi/4$. In Fig. 1 the potential is represented in the unit cell. If g_0 and g_1 are positive and $g_1 \leqslant g_0$ there are four minima at the corners of the cell, one central maximum, and saddle points at the midpoints of the edges. The difference of potential energy between minima and saddle points (i.e., the energy barrier) E_b is given by

$$E_b = 4(g_0 - g_1). \tag{3.2}$$

In the extreme case of very strong x-y coupling ($g_1 = g_0$), the energy barriers vanish and the minima are connected by a network of flat channels (lower panel of Fig. 1). Around the minima, the frequencies related to the curvatures are

$$\omega_a = s_a = \sqrt{2(g_0 - g_1)}, \tag{3.3}$$

at the saddle points the curvature related to ω_c is unstable and we have

$$\omega_c = \sqrt{2(g_0 - g_1)}, \quad s_c = \sqrt{2(g_0 + g_1)}. \tag{3.4}$$

In the presence of x-y coupling, the channel width is not constant; the channel is narrower at the saddle point ($s_a < s_c$).

With the potential (3.1) the quantities (2.26) result:

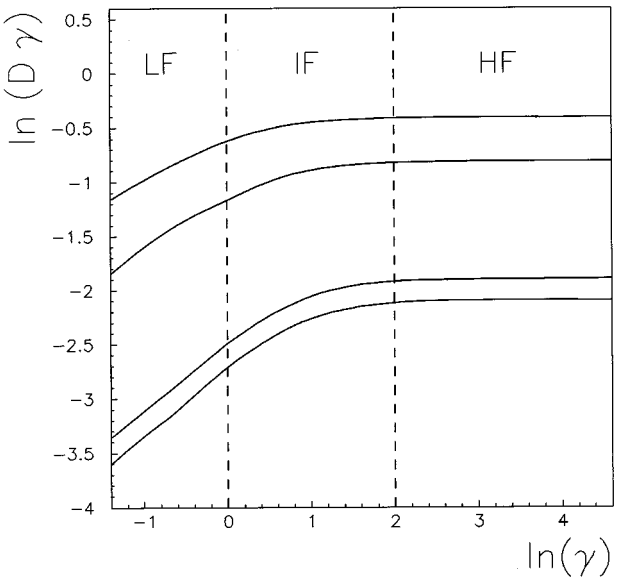

FIG. 2. General behavior of D as a function of γ. The four curves correspond to $g_0 = 0.6$, $g_1 = 0.3$; $g_0 = 1$, $g_1 = 0.5$; $g_0 = 1.4$, $g_1 = 0.4$; and $g_0 = 2$, $g_1 = 1$. Three friction regimes are indicated: high friction (HF), intermediate friction (IF), and low friction (LF).

$$\begin{aligned} F_x^{p-r,h-s} = & -ig_0\delta^{hs}(\delta^{p,r+1} - \delta^{p,r-1}) \\ & + i\frac{g_1}{2}\delta^{h,s+1}(\delta^{p,r+1} - \delta^{p,r-1}) \\ & + i\frac{g_1}{2}\delta^{h,s-1}(\delta^{p,r+1} - \delta^{p,r-1}), \\ F_y^{p-r,h-s} = & -ig_0\delta^{pr}(\delta^{h,s+1} - \delta^{h,s-1}) \\ & + i\frac{g_1}{2}\delta^{p,r+1}(\delta^{h,s+1} - \delta^{h,s-1}) \\ & + i\frac{g_1}{2}\delta^{p,r-1}(\delta^{h,s+1} - \delta^{h,s-1}). \end{aligned} \tag{3.5}$$

With the aid of Eqs. (3.5), (2.21), (2.25), and (2.33) the dynamic structure factor can be evaluated as a function of γ, g_0, and g_1.

IV. RESULTS

The general features of the behavior of the diffusion coefficient with varying friction γ are represented in Fig. 2. The logarithm of $D\gamma = D/D_0$ is plotted as a function of the logarithm of γ at different couples of the potential parameters g_0 and g_1. Three distinct regions can be clearly distinguished, pointing out three friction regimes. Moving from the right to the left, a region is first found where $D\gamma$ is γ independent and therefore D behaves as the inverse friction. This region can be labeled as the high-friction or Smoluchowski regime. Given g_0 and g_1, it is always possible to choose a sufficiently high γ such that the Smoluchowski equation is adequate to describe the dynamics. The Smoluchowski equation can be solved numerically by the MCFM

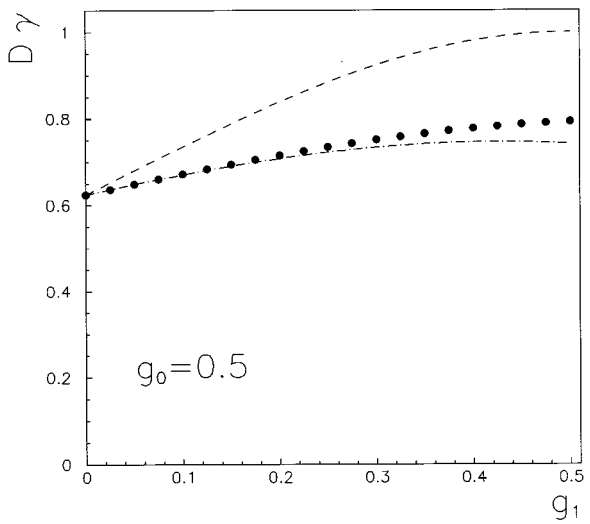

FIG. 3. Diffusion coefficient in the Smoluchowski limit as a function of the x-y coupling g_1 at fixed $g_0=0.5$. The black dots correspond to the exact numerical results; the dashed line to the diffusion-path approximation [Eqs. (4.1)–(4.3)] and the dash-dotted line to D_{Q2} [Eqs. (4.6) and (4.7)].

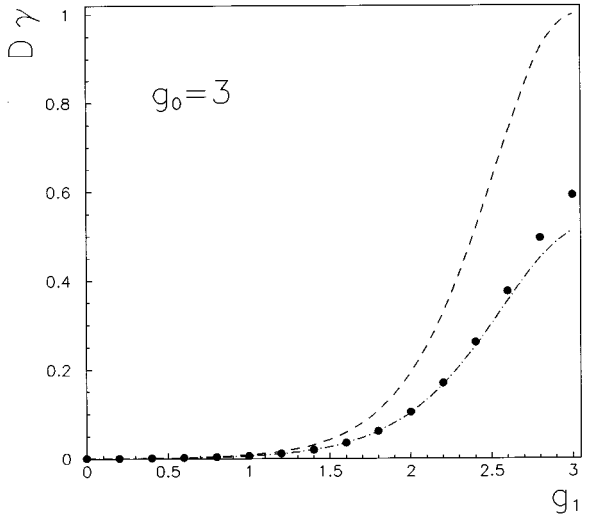

FIG. 4. The same as in Fig. 3, but at higher g_0 ($g_0=3$). The energy barrier E_b ranges from $12k_BT$ (at $g_1=3$) to 0.

too [45]. In the central region, at intermediate values of the friction, $\ln(D\gamma)$ exhibits a knee from a constant value to a decreasing behavior as γ is decreased. This region will be referred to as the intermediate-friction regime and corresponds to the Kramers turnover region. The low-friction regime in the left is characterized by an evident decrease of $\ln(D\gamma)$. As γ takes on lower values, the diffusion coefficient is no longer simply proportional to the inverse friction. Below the knee, the diffusion tends to be energy controlled: the energy of the diffusing particle is almost conserved along the trajectory for long times (of the order of γ^{-1}).

The results for the diffusion coefficient will be presented and discussed separately in the different damping regimes. The exact numerical results will be compared to those of different approximations. The overdamped regime will be examined first.

A. The high-friction regime

As stated above, the overdamped regime is the one in which the probability density in the configuration space can be obtained also by solving the simpler Smoluchowski equation instead of the FPE. The Smoluchowski limit is obtained from the FPE by letting $\gamma\to\infty$ at fixed potential; in this limit $D/D_0=D\gamma$ tends to a constant (see Fig. 2).

In Figs. 3 and 4, $D\gamma$ is studied as a function of the coupling parameter g_1 at fixed g_0. In all the following figures, the 2D FPE exact results will be represented by black dots. D increases with increasing g_1, that is, as the potential goes from the decoupled ($g_1=0$) to the strongly coupled case ($g_1=g_0$). Furthermore, a comparison between Fig. 3 (where $g_0=0.5$) and Fig. 4 ($g_0=2$) shows that, at fixed g_1, the lowest D corresponds to the highest g_0. In all cases the behavior of D is in agreement with the corresponding behavior of the potential barrier E_b [see Eq. (3.2)]. E_b is in fact raised either by increasing g_0 or by decreasing g_1.

The Smoluchowski regime is easier for what concerns analytical calculations. In fact, in 1D, an exact analytical formula for D was obtained a long time ago [13]. In a coupled multidimensional potential an exact formula is not available. However, it is possible to generalize the methods leading to the exact 1D result and to obtain analytical 2D approximations. In the following we treat two different approximations, which are both compared to the exact numerical results.

The first approximation is the DPA. In the DPA, the 2D problem is restricted to a 1D problem by considering the minimum-energy path connecting the wells with the saddle points (which coincides with the x axis in our case). The latter problem is exactly solved at high friction by means of a well-known result [14,15]:

$$D_{\mathrm{DPA}}=\frac{a^2D_0}{\int_0^a dx\,\exp[\beta U(x)]\int_0^a dx\,\exp[-\beta U(x)]}, \tag{4.1}$$

where

$$D_0=k_BT/m\eta, \tag{4.2}$$

$\beta=(k_BT)^{-1}$, and $U(x)=V(x,0)$. In normalized units, $D_0=\gamma^{-1}$ and

$$D_{\mathrm{DPA}}=\frac{1}{\gamma I_0^2(z)}, \tag{4.3}$$

where $I_0(z)$ is the modified Bessel function of order zero [46] and $z=2(g_0-g_1)$.

The second approximation, called in the following the ''quasi-2D'' approximation, can be derived by generalizing to a 2D potential $V(\mathbf{r})$ the method proposed by Günther *et al.* [15] for the 1D case. Here the derivation of the quasi-2D approximation is sketched. When a uniform external force F_0 is applied along the x axis, there will be a mean

velocity v_d in the direction of the force, $v_d=\mu F_0$, where μ is the mobility of the particle. The drift velocity v_d can be calculated as

$$v_d=\frac{\int_{\text{cell}} dydx n(\mathbf{r})v(\mathbf{r})}{\int_{\text{cell}} dydx n(\mathbf{r})}, \tag{4.4}$$

where $n(\mathbf{r})$ is the density of particles, $v(\mathbf{r})$ is the x component of the local velocity, and the integrals are extended over the unit square cell of spacing a. When no external force is applied, the equilibrium density of particles is $n_{\text{eq}}(\mathbf{r})=n_0\exp[-\beta V(\mathbf{r})]$ ($\beta=1/k_BT$). In the presence of a small F_0, $n(\mathbf{r})\simeq n_{\text{eq}}(\mathbf{r})$ and the normalization factor in Eq. (4.4) follows immediately. The evaluation of the numerator is approximated and requires subtler considerations. The integrand is the density of current of particles in the x direction $J(\mathbf{r})=n(\mathbf{r})v(\mathbf{r})$. To perform the integration over the cell, we first keep y fixed and then we integrate over y. Assuming that at fixed y the diffusive motion in the x direction can be treated as one dimensional, $J(\mathbf{r})$ must be x independent along the path, as in the strictly 1D case [15], that is, $J(\mathbf{r})=J(y)$. The further step allowing us to perform the integration over y is the observation that the work done by the external force when the particle moves over a spacing a at fixed y must equal the work dissipated by the friction force acting on the particle:

$$F_0 a=m\eta\int_0^a dx v(\mathbf{r}). \tag{4.5}$$

An expression for v_d follows easily from these considerations; the mobility μ is extracted and, finally, the diffusion coefficient in the quasi-2D approximation D_{Q2} is obtained as $D_{Q2}=k_BT\mu$:

$$D_{Q2}=D_0a^2\frac{\int_0^a dy\left[\int_0^a dx\exp[\beta V(\mathbf{r})]\right]^{-1}}{\int_0^a dy\int_0^a dx\exp[-\beta V(\mathbf{r})]}. \tag{4.6}$$

This expression was derived by Ala-Nissila and Ying [16] by different methods. In normalized units and with the potential (3.1), the quasi-2D approximation gives

$$\gamma D_{Q2}=\frac{\int_0^\pi dy\exp(2g_0\cos y)I_0^{-1}(z)}{\int_0^\pi dy\exp(2g_0\cos y)I_0(z)}, \tag{4.7}$$

where $R=g_1/g_0$, and $z=2g_0(1-R\cos y)$.

Let us compare the approximations with the exact results. In the figures, the DPA corresponds to the dashed lines and D_{Q2} to the dash-dotted lines.

D_{DPA} and D coincide only if $g_1=0$. The 2D decoupled problem splits in fact then into two independent 1D problems. At nonvanishing g_1, D_{DPA} always overestimates the diffusion coefficient and the disagreement becomes more and more important as the x-y coupling is increased (see Figs. 3 and 4). D_{Q2} is a much better approximation, especially at small coupling. In fact, D and D_{Q2} practically coincide when the values of g_1 are small compared with g_0. The difference between D and D_{Q2} becomes more relevant as the coupling parameter g_1 is increased and D_{Q2} always underestimates the diffusion coefficient at every $g_1\neq 0$.

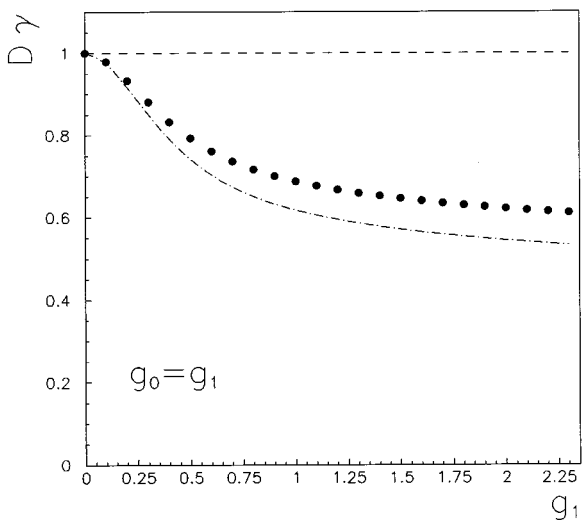

FIG. 5. High-friction diffusion coefficient in the flat-channel case ($g_0=g_1$). Symbols as in Figs. 3 and 4.

Since all approximations are worse at high x-y coupling, we shall examine as a special case the situation of maximum coupling ($g_1=g_0$), corresponding to flat channels. The flat channel gets narrower with increasing g_0 and, consequently, the diffusion coefficient D has a decreasing behavior (see Fig. 5). The DPA gives in this case the constant value $D_{\text{DPA}}=D_0=1/\gamma$, as expected from Einstein's relationship for free diffusion. The quasi-2D approximation instead reproduces the decreasing behavior and gives fairly accurate results. The deviations from the exact result are not very large up to the highest values of g_1 reported in Fig. 5. Anyway, a more accurate investigation at high couplings will now be carried on.

The asymptotic behavior of D_{Q2} at very high couplings in the flat channel case can be evaluated from Eq. (4.7) taking the limit $g_1\to\infty$ when $g_1=g_0$. It can be shown that $D_{Q2}\gamma$ vanishes as

$$D_{Q2}\gamma=\frac{1}{A+B\ln g_1}. \tag{4.8}$$

The coefficients A and B can be extracted from the data in Fig. 6; it turns out that $A=1.70$, $B=0.250$.

In Fig. 6, both $(D\gamma)^{-1}$ and $(D_{Q2}\gamma)^{-1}$ are plotted as a function of $\ln g_1$ ($g_1=g_0$). The behavior of $(D_{Q2}\gamma)^{-1}$ is, as expected, linear in $\ln g_1$ at high g_1. What is more interesting, however, is the result concerning the exact diffusion coefficient in the limit of very high x-y coupling. From the results in Fig. 6, $(D\gamma)^{-1}$ also appears to have an asymptotic logarithmic dependence on the coupling g_1. This suggests that $D\gamma$ should vanish in the limit of infinite coupling in the same way as D_{Q2}. Assuming that the asymptotic behavior of $D\gamma$ is also given by Eq. (4.8), the parameters A and B can be extracted from the data in Fig. 6. It turns out that $A=1.48$,

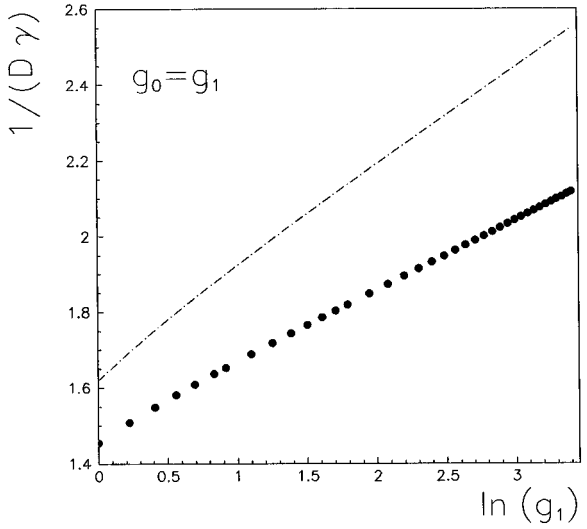

FIG. 6. Asymptotic behavior of the inverse diffusion coefficient at high friction in the flat-channel case ($g_0=g_1$). D_{Q2} (dash-dotted line) vanishes as in Eq. (4.8) at high g_1; the exact numerical results display the same kind of behavior.

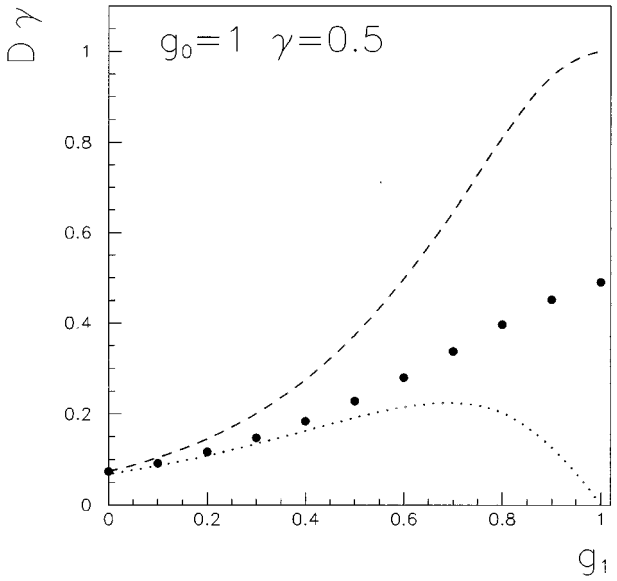

FIG. 7. Diffusion coefficient at intermediate friction ($\gamma=0.5$) as a function of the x-y coupling g_1 at fixed $g_0=1$. The black dots correspond to the exact numerical results; the dashed line to the diffusion-path approximation [Eqs. (4.1)–(4.3)] and the dotted line to D_{JM} [Eq. (4.12)].

$B=0.186$. From these values, it follows that the ratio D_{Q2}/D should tend to the asymptotic limit $D_{Q2}/D=0.744$. The DPA approximation, instead, gives in the flat-channel case the coupling-independent result $D_{\mathrm{DPA}}\gamma=1$ and is therefore asymptotically wrong at high x-y couplings.

A diffusion problem with some similarity with our flat-channel case was studied by Zwanzig [47], who considered the high-friction motion of a Brownian particle in a 2D channel with periodically varying width. In the case considered by Zwanzig, no potential is present in the channel and the particle is subjected only to the geometrical constraint of a nonconstant channel width. The effective diffusion coefficient is always smaller than Einstein's relationship. Einstein's result is recovered exclusively for a rectangular channel. In fact, when the channel width changes periodically along the x direction, the particle can wander along the y direction before finding its way through the ''bottlenecks.'' This makes the motion in the x direction slower and therefore the diffusion coefficient is smaller. Our results for motion in a flat channel are qualitatively in agreement with the results obtained by Zwanzig, as the diffusion coefficient is always lowered with respect to the result given by the Einstein relation [Eq. (4.2)].

B. The intermediate- and low-friction regimes

In this section we will present the results for the diffusion coefficient in the intermediate- and low-friction regimes.

The effect of the x-y coupling at a fixed γ is first examined. At moderate damping ($\gamma=0.5$), $D\gamma$ (black dots in Fig. 7) has the same qualitative behavior at fixed g_0 ($g_0=1$) as in the high-friction regime. D increases as the coupling parameter g_1 varies from 0 to g_0, that is as the potential barrier E_b [Eq. (3.2)] goes from its maximum value $4g_0$ to 0, respectively.

At fixed g_0 and g_1, an accurate investigation of the diffusion coefficient as a function of the friction is presented in Fig. 8. The potential barrier is rather high, $E_b=4k_BT$ ($g_0=1.5$, $g_1=0.5$) and $D\gamma$ is always less than one, as is to be expected since $D\gamma$ is the ratio between the diffusion coefficient and Einstein's free diffusion coefficient. A strong decrease is shown going towards the lowest values of γ. At the highest γ's, say $\gamma\geqslant 5$, $D\gamma$ tends to a constant value; therefore D behaves like $1/\gamma$ towards the moderate-high friction values.

The diffusion along a flat channel is examined, as at high damping, as a particular case. In Figs. 9 and 10 all symbols

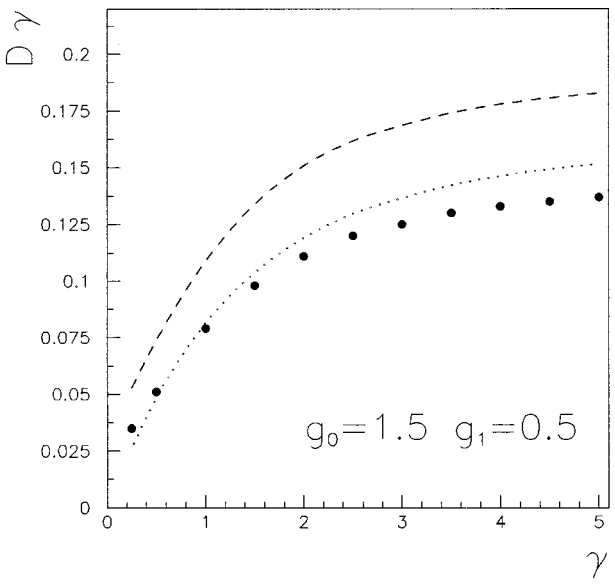

FIG. 8. Diffusion coefficient as a function of the friction γ in the turnover region and below. g_0 and g_1 are chosen to give a sufficiently high-energy barrier ($E_b=4k_BT$) that the jump-diffusion regime holds. Symbols as in Fig. 7.

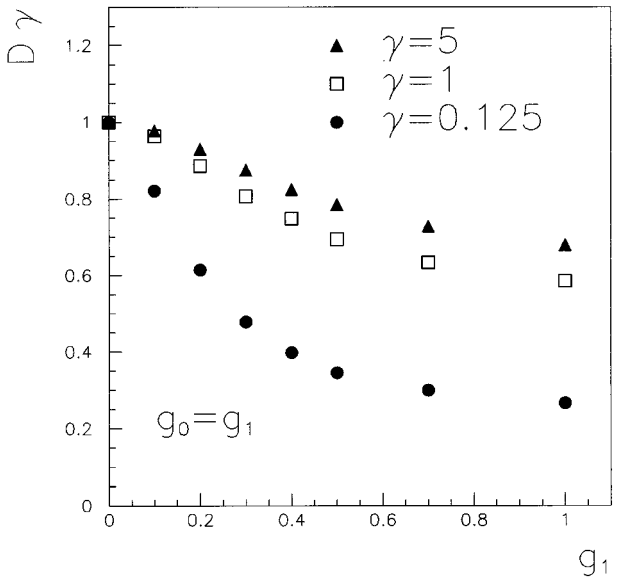

FIG. 9. Diffusion coefficient in the flat-channel case ($g_0=g_1$) as a function of g_1. The different symbols correspond to three values of the friction γ, as indicated in the figure.

refer to the exact numerical results. In Fig. 9, the effect of raising $g_1=g_0$, that is, of narrowing the channel, is studied at three different values of γ ($\gamma=0.125$, $\gamma=1$, $\gamma=5$). $D\gamma$ is correspondingly found to have a decreasing behavior. At nonvanishing g_1, $D\gamma$ is smaller than Einstein's value, and the strongest differences are obtained at the lowest friction.

In Fig. 10, $D\gamma$ is plotted as a function of the friction at three different values of the parameter g_0 (black dots: $g_0=g_1=0.5$, squares: $g_0=g_1=0.7$; open circles: $g_0=g_1=1$). As in Fig. 8, D behaves as the inverse power of the friction at the highest dampings and rapidly decreases with decreasing friction. At the same γ, the lowest values of

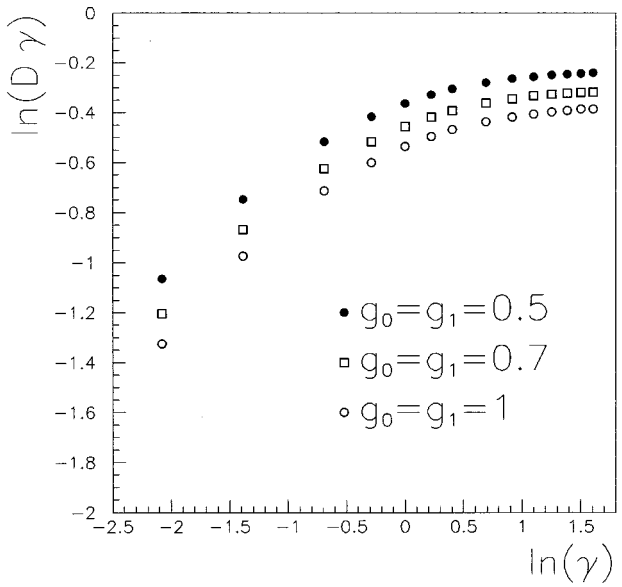

FIG. 10. Diffusion coefficient in the flat-channel case ($g_0=g_1$) as a function of γ. The different symbols correspond to three values of g_1, as indicated in the figure.

$D\gamma$ are obtained at the highest g_0, i.e., when the channel is narrower.

The presence of an x-y coupling therefore has the effect of making the diffusive motion slower. The diffusion coefficient is smaller and this is more evident at low friction. In fact, in the coupled case, long straight trajectories are less favored than in the decoupled case. The effect is evident even at small couplings.

The coupled potential (3.1) has been studied by different groups [29,30] in the investigation of chaotic diffusion in Hamiltonian systems. They noticed that without the coupling term, the corresponding Hamiltonian is integrable and no diffusive and chaotic motion is observed. The presence of the coupling allows instead an energy exchange between the x and y degrees of freedom. This happens however small the coupling is and the results remain qualitatively unchanged, as long as the coupling is different from zero [29]. In the presence of coupling, either ''normal'' or ''anomalous'' diffusion can take place, according to the strength of the coupling, although the system is conservative. Their considerations cannot of course be directly compared with the results we have presented in this paper, since we are dealing with a different problem: in Refs. [29,30] diffusion arises deterministically, while here the diffusive motion is due to random and friction forces. It is anyway worth noticing that our nonconservative system, in the limit $\gamma\rightarrow 0$, is equivalent to an ensemble of conservative systems, whose weights are given by Boltzmann factors.

In the low-damping regime no exact analytical 2D results are available; even in 1D, in the low-friction expansion of the solution of the 1D FPE [3], only the leading terms are known analytically, providing a good approximation exclusively at extremely low damping [6]. Approximations for the 2D diffusion coefficient are provided, anyway, by the DPA and the 2D-jump model. In the following we will discuss these approximations and their validity as resulting from the comparison with FPE 2D exact results.

As said in the Introduction, the DPA is not restricted *a priori* to a particular range of the friction or of the potential amplitudes. The one-dimensional diffusion coefficient $D_{\rm DPA}$ can be obtained solving the FPE in the effective 1D potential experienced by the diffusing particle if the motion could be restricted only to the most favorable trajectory that is in our case $U(x)=V(x,0)$. The resulting 1D problem is then numerically solved. The details of the method leading to the solution of the FPE with a 1D potential have been published elsewhere [6]; here we only recall that the computing efforts are far lighter in the 1D case than in two coupled dimensions.

DPA results have been compared with D at intermediate and low friction, too, and, as in the previous high-friction figures, they are represented by a dashed line. As in the high-friction case, $D_{\rm DPA}$ overestimates the diffusion coefficient; the deviations are even more relevant (compare Fig. 7 with Figs. 3 and 4). In fact, the DPA gives worse and worse results with decreasing friction. This is evident from Fig. 8 and panel (a) of Fig. 11, where the relative difference $C_{\rm DPA}=(D_{\rm DPA}-D)/D$ is plotted as a function of γ. $C_{\rm DPA}$ is nearly independent of γ at the highest-friction values (in the case presented here, it is about 0.3) but it strongly increases when $\gamma<0.5$. The DPA can therefore lead to relevant errors

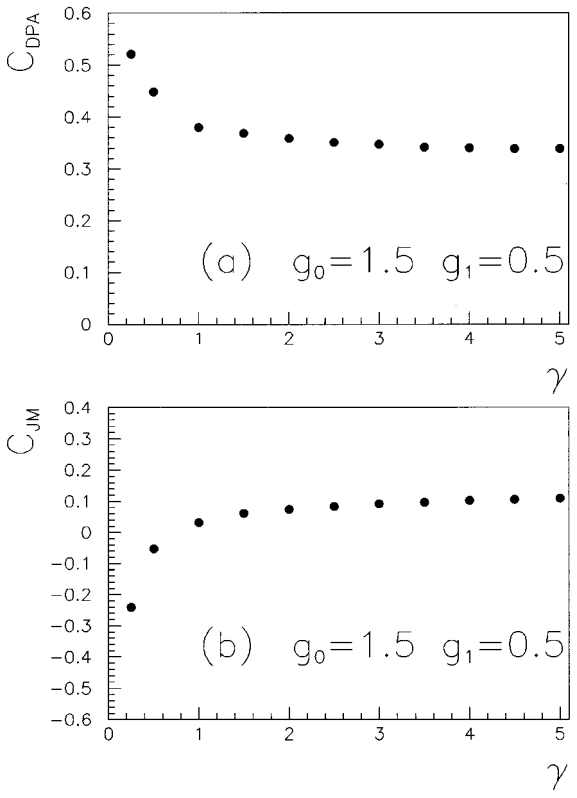

FIG. 11. Relative errors $C_{\mathrm{DPA}}=(D_{\mathrm{DPA}}-D)/D$ and $C_{\mathrm{JM}}=(D_{\mathrm{JM}}-D)/D$ at fixed g_0 and g_1 as functions of the friction.

at low friction. The disagreement with the DPA is even more important for flat channels (Figs. 9 and 10) where $D_{\mathrm{DPA}}\gamma=1$ at every friction. As an example, at the lowest friction considered here, $\gamma=0.125$, we obtained $D\gamma=0.27$ at $g_0=g_1=1$; the DPA would then lead to an error of about a factor 4.

We can conclude that at low damping the DPA overestimates the diffusion coefficient more dramatically than in the high-friction regime. Dimensional effects become more and more important with decreasing friction, and cannot be neglected at all for γ below the turnover (typically placed between $\gamma=1$ and $\gamma=0.5$) even at small coupling.

As mentioned in the Introduction, the hopping model [42] is the standard approach to diffusion [25,39,40]. The 2D-jump model provides a good description of the migration mechanism at high potential barriers. In this picture the diffusion coefficient is given by

$$D=\tfrac{1}{4}\langle l^2\rangle r_j=\langle l^2\rangle r_j^{(1)}, \tag{4.9}$$

where $\langle l^2\rangle$ is the mean-square jump length, r_j is the total jump rate taking into account the four different escape directions, and $r_j^{(1)}$ is the directional escape rate over a saddle point. Equation (4.9) is correct at high barriers, independently of the friction, but r_j and $\langle l^2\rangle$ cannot be evaluated *a priori* in every friction regime. If the friction is not too low, one can expect that the diffusive motion consists of hops between nearest-neighbor lattice sites (single jumps) and $\langle l^2\rangle$ is simply given by the squared lattice spacing

$$\langle l^2\rangle\simeq a^2, \tag{4.10}$$

but at low damping long jumps become important [6,7,33,41,48] and the evaluation of $\langle l^2\rangle$ is not trivial [25,33]. The directional rate $r_j^{(1)}$ can be approximated by a 2D extension of Kramers's [44] high-friction result [11,17,18,43]:

$$r_j^{(1)}=\frac{1}{2\pi}\frac{\omega_a s_a}{s_c}\left[\sqrt{1+\frac{\gamma^2}{4\omega_c^2}}-\frac{\gamma}{2\omega_c}\right]\exp(-E_b). \tag{4.11}$$

In Eq. (4.11) E_b is the dimensionless potential barrier and ω_a, s_a and ω_c, s_c are the vibrational frequencies related to the curvatures of the potential near the minimum and near the saddle point, respectively. The validity of Eq. (4.11) is not limited to the Smoluchowski limit but it can be extended down to values of the friction around the turnover. Taking into account these results and Eqs. (3.2)–(3.4), the diffusion coefficient in the jump model (JM) is finally obtained as

$$D_{\mathrm{JM}}=\pi^2 r_j=2\sqrt{2}\pi\frac{g_0-g_1}{\sqrt{g_0+g_1}}\left[\sqrt{1+\frac{\gamma^2}{8(g_0-g_1)}}-\frac{\gamma}{\sqrt{8(g_0-g_1)}}\right]\exp[-4(g_0-g_1)]. \tag{4.12}$$

In the limit of infinite friction, the formula provided by the JM coincides with the high-barrier limit of the quasi-2D approximation [Eq. (4.7)].

D_{JM} is represented in Figs. 7 and 8 by a dotted line. Figure 7 shows that Eq. (4.12) is appropriate even at intermediate friction ($\gamma=0.5$), as long as the potential barriers are sufficiently high. From our results, D_{JM} can be considered a reasonable approximation when $g_0-g_1\geqslant 0.5$. If this difference becomes smaller, i.e., at $E_b\leqslant 2k_BT$, Eq. (4.12) can no longer be correct, as shown by the same authors in the 1D case [25], both by numerical calculations and by qualitative arguments about some typical time scales.

Considerations about the range of validity of the hopping description develop also from an examination of Fig. 12, where the logarithm of the exact diffusion coefficient D is plotted as a function of the potential barrier E_b. Both γ and g_0 are fixed ($\gamma=0.5$, $g_0=1$). According to the usual phenomenological Arrhenius law

$$D=D_A\exp(-E_b), \tag{4.13}$$

where D_A is a prefactor weakly dependent on temperature. If $\ln D$ is plotted as a function of E_b, a linear behavior is expected at least in a limited range of temperatures. Figure 12 shows that at low barriers significant deviations from the Arrhenius law are possible and the diffusion may become unactivated. In this case the model of migration taking place by activated hops is certainly not appropriate. The linear behavior of $\ln D$, and therefore the JM, is recovered only at high barriers.

At a fixed and high potential barrier, D_{JM} is a worse approximation as the friction is decreased, as shown in Fig. 8 and stressed in panel (b) of Fig. 11, where the relative difference $C_{\mathrm{JM}}=(D_{\mathrm{JM}}-D)/D$ is represented. The deviations of D_{JM} from the exact result are to be imputed both to the poor evaluation of $r_j^{(1)}$ and of $\langle l^2\rangle$ in Eq. (4.9). The estimation

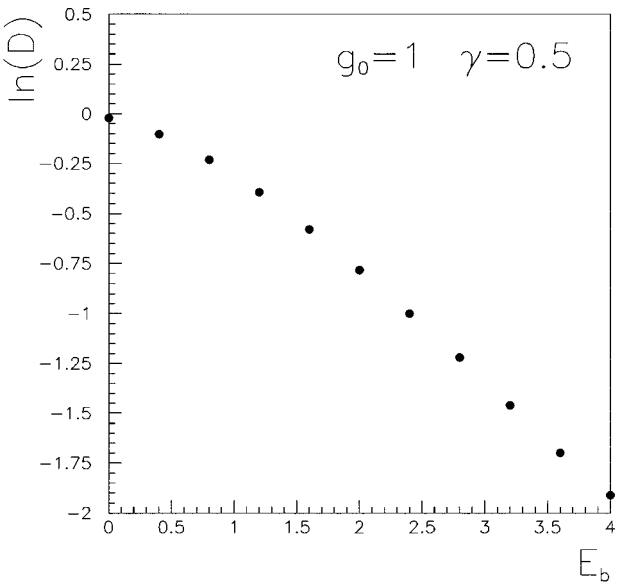

FIG. 12. Arrhenius plot of the diffusion coefficient at intermediate friction ($\gamma=0.5$).

(4.11) for $r_j^{(1)}$ loses its validity at low friction, and at the same time the evaluation of the mean-square jump length is far more complicated than Eq. (4.10) in the low-damping regime, where the particle can jump over more than one lattice spacing.

Finally, a few words about the computational effort required for the evaluation of D. The number of iterations in the matrix continued fraction (2.33) increases towards low γ; larger matrices are needed both with decreasing γ and with increasing g_0+g_1. For instance, the following truncations [see Eq. (2.28)] are sufficient for a precision better than 1%: at $g_0=2$, $g_1=1$, and $\gamma=1000$ $P=H=8$, $N=1$ and one iteration in the continued fraction; at $g_0=0.6$, $g_1=0.3$, and $\gamma=1000$ $P=H=5$, $N=1$ and one iteration; at $g_0=0.6$, $g_1=0.3$, and $\gamma=1$ $P=H=5$, $N=6$ and six iterations.

V. CONCLUSIONS

Our motivation for the present work was twofold. First, we intended to study the dynamics of nonlinear 2D periodic systems in the dissipative case. The nonlinear dynamics of a classical particle moving conservatively in a 2D field of force exhibits chaos and enhanced diffusion [29,30]; these dynamical features do not survive in the more realistic case of noise-assisted diffusion, but the investigation of the very-low-friction regime remains of great interest. Secondly we wanted to extend to 2D the Fokker-Planck model of adatom surface diffusion [6,32,33,36,41,49]. Adatom diffusion on crystal surfaces is obviously a multidimensional problem and at least two coupled dimensions must be taken into account to study dimensional effects. Moreover both experiments and molecular dynamics simulations indicated that typical friction values are around and below the Kramers turnover (the knee region in Fig. 2). So the dynamical investigation must cover a wide damping range in order to give a reasonable description of surface diffusion.

In this paper we have presented a detailed investigation of the noise-activated diffusion of a classical particle moving in a two-dimensional coupled periodic potential on a square lattice. The Fokker-Planck equation has been numerically solved and the diffusion coefficient has been calculated in a wide range of theory parameters: the strength of the friction, the x-y coupling parameter, and the amplitude of the potential barriers along the diffusion path. At high friction, results are easily obtained by the MCFM up to barriers of $10k_BT$ and more (see Fig. 4, for instance) and with strong coupling (see Fig. 6). We stress that, for our model potential, the stronger is the coupling the lower is the barrier (which is proportional to g_0-g_1); the computational effort increases with the sum g_0+g_1. The calculations become cumbersome at lower friction. However, it is possible to explore the jump-diffusion regime (at $E_b\simeq 4k_BT-5k_BT$) well below the turnover point, down to a friction regime (around $\gamma=0.1$) where the single-jump model is no longer correct and long jumps should be likely. A shortcoming of our numerical method is that, at low friction, barriers greater than $4k_BT-5k_BT$ cannot be studied by a reasonable computational effort. Many systems in surface diffusion are characterized by higher barriers at the temperatures of the experiments; however there are several systems which present rather low barriers [for instance, Na/Cu(100) [34], CO on different faces of Ni and Pt, noble gases on metals, etc. [50]], which are of few k_BT at room temperature or somewhat above.

Numerical results have been obtained for the egg-carton potential which may be considered representative of the large class of potentials where the more favorable diffusion trajectories are straight lines. In particular, both high and low friction have been considered; the effect of the x-y coupling has been discussed in detail. At high friction, the exact numerical results have been compared to those of two analytical approximations: the diffusion-path and the quasi-2D approximation. The diffusion-path approximation reduces the 2D problem to one dimension and neglects the effect of the x-y coupling; it turns out that this approximation strongly overestimates the diffusion coefficient at large couplings. For instance, in the case of a flat channel, the diffusion-path approximation reduces to the Einstein relation and does not depend on the coupling while the exact result tends to zero in the limit of infinite coupling. On the contrary, the quasi-2D approximation always gives rather good results, even in the case of extremely strong coupling. The quasi-2D approximation has been derived by fixing the value of one coordinate and by solving the diffusion problem along the other coordinate as if it were strictly one dimensional. This is expected to be essentially correct if all important diffusion trajectories occur on straight lines. Therefore the quasi-2D approximation is expected to give good results when the minima and the saddle points lie on straight lines, as it happens in the lattice considered in the present paper. In a honeycomb lattice [51,52], this is not the case and one could expect a worse agreement between the quasi-2D approximation and the exact data.

At intermediate and low friction the effect of the coupling is even stronger in reducing the diffusion coefficient; thus the diffusion-path approximation is not reliable even at small couplings. In the presence of coupling, it is difficult for the diffusing particle to perform long and straight inertial trajectories: the coupling allows the energy transfer between the x and y degrees of freedom. More intuitively, in our model

potential, the channel width is smaller at the saddle points than at the minima and this reduces the possibility of long straight flights. In these regimes, there are no good analytical estimates covering the full parameter range. At high potential barriers, it is possible to compare the exact results with those of the jump-diffusion model; the latter is satisfactory down to the turnover region. Below the turnover, long jumps are activated and the mean-square jump length cannot be easily evaluated; neglecting long jumps strongly underestimates the diffusion coefficient.

Finally, we remark that the numerical method developed in this paper can be easily generalized to position-dependent friction and tilted potentials [6,27]. In the same framework, different classes of kinetic equations, such as the linearized Boltzmann equation with Bhatnagar-Gross-Krook kernel [53] or Skinner-Wolynes equations [54], can be treated [3,55]. Our method leads to exact numerical results, which may be used to test analytical or numerical approximations obtained by different methods (for instance, finite-barrier corrections [56]). The method gives the full dynamic structure factor, from which all relevant correlation functions, the escape rate, and the jump-probability distribution can be derived [7]. At low friction and high barriers the MCFM becomes inefficient; the investigation of noise-activated diffusion in this regime is still an open problem and the development of different methods (e.g., Langevin simulations, reactive-flux method) may be useful.

[1] *Noise in Nonlinear Systems*, edited by F. Moss and P.V.E. McClintock (Cambridge University Press, Cambridge, England, 1989).

[2] C.W. Gardiner, *Handbook of Stochastic Methods* (Springer-Verlag, Berlin, 1990).

[3] H. Risken, *The Fokker-Planck Equation* (Springer, Berlin, 1989).

[4] V.I. Mel'nikov, Phys. Rep. **209**, 1 (1991).

[5] G.J. Moro and A. Polimeno, Chem. Phys. Lett. **189**, 133 (1992).

[6] R. Ferrando, R. Spadacini, and G.E. Tommei, Surf. Sci. **265**, 273 (1992).

[7] R. Ferrando, R. Spadacini, and G.E. Tommei, Phys. Rev. E **48**, 2437 (1993).

[8] Y. Georgievskii and E. Pollak, Phys. Rev. E **49**, 5098 (1994); Y. Georgievskii, M.A. Kozhushner, and E. Pollak, J. Chem. Phys. **102**, 6908 (1995).

[9] M.O. Magnasco, Phys. Rev. Lett. **71**, 1477 (1993).

[10] P. Reimann, Phys. Rev. Lett. **74**, 4576 (1995).

[11] P. Hänggi, P. Talkner, and M. Borkovec, Rev. Mod. Phys. **62**, 251 (1990).

[12] P. Jung, Phys. Rep. **234**, 175 (1993).

[13] R. Landauer, in *Noise in Nonlinear Systems*, edited by F. Moss and P.V.E. McClintock (Cambridge University Press, Cambridge, England, 1989), Vol. I.

[14] S. Lifson and J.L. Jackson, J. Chem. Phys. **36**, 2410 (1962); R. Festa and E. Galleani d'Agliano, Physica A **90**, 229 (1978).

[15] L. Günther, M. Revzen, and A. Ron, Physica A **95**, 367 (1979).

[16] T. Ala-Nissila and S.C. Ying, Phys. Rev. Lett. **65**, 879 (1990); Prog. Surf. Sci. **39**, 227 (1992).

[17] J.R. Banavar, M.H. Cohen, and R. Gomer, Surf. Sci. **107**, 113 (1981).

[18] J.S. Langer, Ann. Phys. (N.Y.) **54**, 258 (1969).

[19] A. Nitzan, J. Chem. Phys. **86**, 2734 (1987).

[20] E. Pollak and E. Hershowitz, Chem. Phys. **180**, 191 (1994).

[21] J.E. Straub and B.J. Berne, J. Chem. Phys. **85**, 2999 (1986).

[22] R. Kubo, Rep. Prog. Phys. **29**, 255 (1966).

[23] H.D. Vollmer and H. Risken, Physica A **110**, 106 (1982); Mol. Phys. **46**, 555 (1982).

[24] J.P. Hansen and I.R. McDonald, *Theory of Simple Liquids* (Academic Press, London, 1976).

[25] R. Ferrando, R. Spadacini, G.E. Tommei, and G. Caratti, Physica A **195**, 506 (1993).

[26] R. Ferrando, R. Spadacini, and G.E. Tommei, Phys. Rev. A **46**, 699 (1992).

[27] R. Ferrando, R. Spadacini, and G.E. Tommei, Phys. Rev. E **51**, 126 (1995).

[28] A. Igarashi and T. Munakata, J. Phys. Soc. Jpn. **57**, 2439 (1988).

[29] T. Geisel, A. Zacherl, and G. Radons, Phys. Rev. Lett. **59**, 2503 (1987); Z. Phys. B **71**, 117 (1988).

[30] J. Klafter and G. Zumofen, Phys. Rev. E **49**, 4873 (1994).

[31] L.Y. Chen and S.C. Ying, Phys. Rev. B **49**, 13 838 (1994).

[32] R. Ferrando, R. Spadacini, and G.E. Tommei, Surf. Sci. **251/252**, 773 (1991); Phys. Rev. B **45**, 444 (1992).

[33] R. Ferrando, R. Spadacini, G.E. Tommei, and G. Caratti, Surf. Sci. **311**, 411 (1994).

[34] J. Ellis and J.P. Toennies, Phys. Rev. Lett. **70**, 2118 (1993).

[35] E. Ganz, S.K. Theiss, I.S. Hwang, and J. Golovchenko, Phys. Rev. Lett. **68**, 1567 (1992); D.C. Senft and G. Ehrlich, *ibid.* **74**, 294 (1995).

[36] L.Y. Chen and S.C. Ying, Phys. Rev. Lett. **71**, 4361 (1993).

[37] K.D. Dobbs and D.J. Doren, J. Chem. Phys. **97**, 3722 (1992).

[38] J.C. Tully, G.H. Gilmer, and M. Shugard, J. Chem. Phys. **71**, 1630 (1979).

[39] D.E. Sanders and A.E. DePristo, Surf. Sci. Lett. **264**, L169 (1992).

[40] R. Ferrando, R. Spadacini, and G.E. Tommei, Surf. Sci. **287/288**, 886 (1993).

[41] A.S. Prostnev, M.A. Kozhushner, and B.R. Shub, Surf. Sci. **336**, 385 (1995).

[42] C.T. Chudley and R.J. Elliott, Proc. Phys. Soc. London **77**, 353 (1961).

[43] R.J. Donnelly and P.H. Roberts, Proc. R. Soc. London Ser. A **312**, 519 (1969).

[44] H.A. Kramers, Physica **7**, 284 (1940).

[45] G. Caratti, R. Ferrando, R. Spadacini, and G.E. Tommei (unpublished).

[46] M. Abramowitz and I.A. Stegun, *Handbook of Mathematical Functions* (Dover, New York, 1972).

[47] R. Zwanzig, Physica A **117**, 277 (1983).

[48] G. Wahnström, J. Chem. Phys. **84**, 5931 (1986).

[49] R. Tsekov and E. Ruckenstein, Surf. Sci. **344**, 175 (1995).

[50] E.G. Seebauer and C.E. Allen, Prog. Surf. Sci. **49**, 265 (1995), and references therein.
[51] B. Bagchi, R. Zwanzig, and M.C. Marchetti, Phys. Rev. A **31**, 892 (1985).
[52] D.S. Sholl and R.T. Skodje, Physica D **71**, 168 (1994).
[53] P.L. Bhatnagar, E.P. Gross, and M. Krook, Phys. Rev. **94**, 511 (1954).
[54] J.L. Skinner and P.G. Wolynes, J. Chem. Phys. **69**, 2143 (1978); **72**, 4913 (1980).
[55] R. Ferrando, R. Spadacini, and G.E. Tommei, Chem. Phys. Lett. **202**, 248 (1993).
[56] P. Talkner and E. Pollak, Phys. Rev. E **47**, 21 (1993); R. Ferrando, R. Spadacini, G.E. Tommei, and V.I. Mel'nikov, *ibid.* **51**, 1645 (1995).